Pulsed laser deposition of thin films of ($La_{1-x}Ca_x$)MnO_3

1996 J. Phys.: Condens. Matter 8 10737

(http://iopscience.iop.org/0953-8984/8/49/057)

J. Phys.: Condens. Matter **8** (1996) 10737–10752. Printed in the UK

Pulsed laser deposition of thin films of $(La_{1-x}Ca_x)MnO_3$

J F Lawler†, J M D Coey, J G Lunney and V Skumryev‡
Department of Physics, Trinity College, Dublin 2, Ireland

Received 19 December 1995, in final form 23 July 1996

Abstract. Manganites of the series $(La_{1-x}Ca_x)MnO_3$, with $x = 0, 0.1, 0.3, 0.5, 0.7$ and 1.0, have been characterized in ceramic form and thin films have been prepared by pulsed laser deposition. Characterization techniques included x-ray diffraction, conductivity and magnetoresistance, magnetization and susceptibility, optical spectroscopy and the Faraday effect. Both the films and ceramics exhibit a maximum low-temperature conductivity at $x \approx 0.3$ which is coexistent with ferromagnetic order. The negative magnetoresistance effect is qualitatively different for the $x = 0.3$ and $x = 0.5$ compositions. For $x = 0.3$ the magnetoresistance peak occurs around the Curie point, whereas for $x = 0.5$ the onset of magnetoresistance is somewhat below T_c and increases monotonically as $T \to 0$. The applied field appears to modify the magnetic order (on the scale of the spin diffusion length) down to the lowest temperatures for $x = 0.5$, but for $x = 0.3$ the ferromagnetic order is essentially complete and collinear below the Curie point.

1. Introduction

The electrical and magnetic properties of the perovskite manganite series $(La_{1-x}A_x)MnO_3$ (A is a divalent ion like Ca, Sr or Ba) were first investigated in the 1950s [1]. Starting from an insulating antiferromagnet ($x \approx 0$) the resistivity drops with increased doping, concurrent with a progressive change from planar antiferromagnetic to ferromagnetic order. The magnetization is maximized for values of $x \approx 0.3$, for which it reaches a value close to the spin-only value expected for a ferromagnetic mixture of $Mn^{3+}(3d^4)$ and $Mn^{4+}(3d^3)$ ions. This composition, which gives the highest Curie temperature, also gives the lowest resistivity when the conduction becomes metallic (temperature-independent) in character below the Curie point. At higher doping ($x > 0.5$) the ferromagnetism disappears and the compound returns to an antiferromagnetic insulating form. This unusual behaviour was first explained in terms of the double-exchange interaction by Zener [2], whereby electron hopping with spin memory in the manganese $e_g \uparrow$ band simultaneously produces ferromagnetic ordering and a high conductivity. A more detailed theoretical description of this interaction was given by Anderson and Hasegawa [3] and it was applied to the $(La_{1-x}Ca_x)MnO_3$ system by de Gennes [4]. Non-stoichiometry, in the form of cation deficiency, also formally introduces Mn^{4+} ions and it has a similar effect on the magnetic order but not on the electrical properties [5].

The generic crystal structure of perovskite is shown in figure 1(a). The oxides rarely have such a simple unit cell. The misfit of the cation radii in relation to the sizes of the interstices in a cubic close-packed oxygen lattice often leads to an orthorhombic (O)

† Present address: Faculty of Science, University of Nijmegen, The Netherlands.
‡ Permanent address: Department of Solid State Physics, Sofia University, Bulgaria.

0953-8984/96/4910737+16$19.50

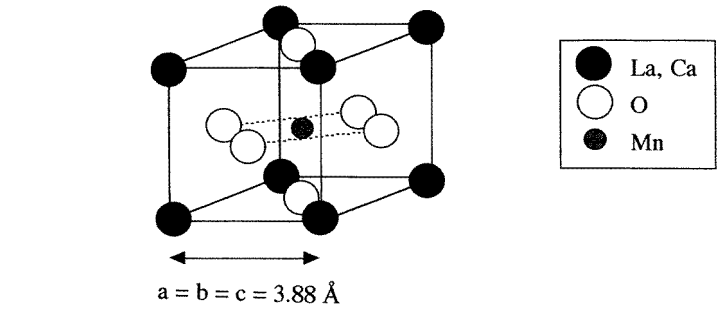

(a)

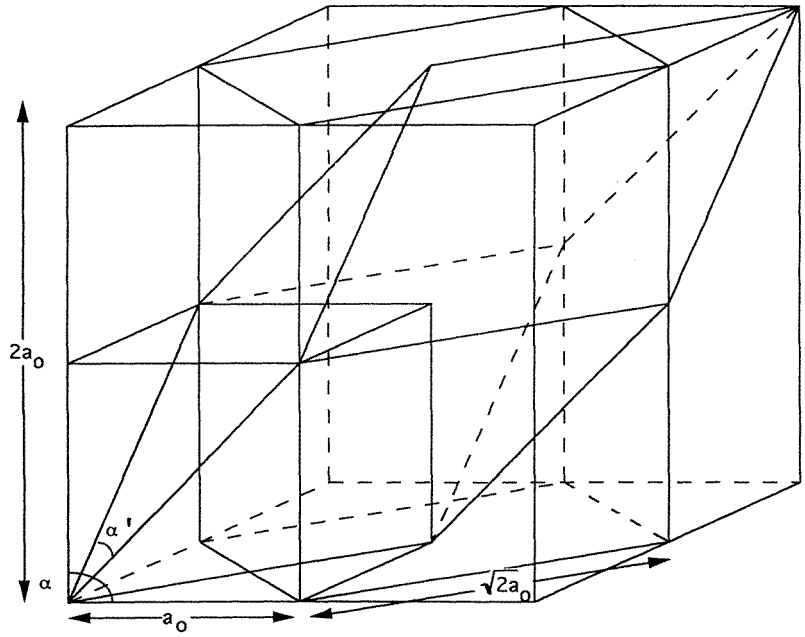

(b)

Figure 1. (a) The ideal crystal structure of perovskite (b) A sketch showing the relationships among the primitive perovskite, orthorhombic, monoclinic and doubled perovskite unit cells.

distortion ($GdFeO_3$ structure). In the undoped $LaMnO_3$ there is further orthorhombic (O′) Jahn–Teller distortion of the structure due to the Mn^{3+} ion ($3d^4$). In the *a*–*c* plane the spins of the Mn^{3+} ions lie along the *b* axis and are coupled parallel in the plane; but successive planes are coupled antiparallel, giving the planar antiferromagnetic structure. With increased doping the moments tilt towards the *c* axis producing ferromagnetic order [4]. At higher doping the structure goes through a series of antiferromagnetic charge-ordered superstructures before reverting to a cubic-type structure for pure $CaMnO_3$ [6]. So starting from the insulating $LaMnO_3$, the replacement of Ca^{2+} for La^{3+} creates d holes in an e_g (σ^*) band which may hop among the equivalent manganese positions around the Ca ions. This causes a re-configuration of the oxygen ions around the manganese with a hole since Mn^{4+} (d^3) is not a Jahn–Teller ion. The magnetic moments of the manganese ions between

which the hole hops tend to be ferromagnetic. For low Ca content ($x < 0.1$) the hole is strongly bound to the sites neighbouring the Ca^{2+} ion and it cannot propagate throughout the lattice. A bound ferromagnetic polaron is thus formed. For higher concentrations the ferromagnetic polarons begin to interact since holes can percolate through the crystal via sites neighbouring the Ca ions. At the same time the hopping energy to move from one site to another decreases, as the Jahn–Teller stabilization energy decreases and thus the hopping rate of the hole becomes more rapid with increasing x. This has been directly confirmed by NMR measurements [7]. The strength of the ferromagnetic interaction increases with x and the interaction between ferromagnetic polarons is also ferromagnetic and simultaneously gives rise to an increase in conductivity. The polarons lose their identity at $x \approx 0.3$, where the whole lattice becomes a collinear ferromagnet.

The perovskite manganites, especially the end member, have the ability to accommodate random cation vacancies and the compound is more correctly described by the formula $(La_{1-\delta}Mn_{1-\delta})O_3$ [8], where δ is typically less than 0.05. The formal oxygen excess and the Jahn–Teller distortion give rise to a range of different though related structures as a function of δ [9] and these will be discussed later in relation to the properties of the ceramic materials. It should be emphasized that the manganites exist over a range of oxygen stoichiometry [9] which takes the form of cation vacancies both on La and on Mn sublattices at ambient oxygen pressure [10] and the physical properties of the $x = 0$ end member are particularly sensitive to the cation/oxygen ratio [5]. The parent compound may be indexed on a slightly orthorhombic cell with $a \approx b \approx \sqrt{2}a_0$ and $c = 2a_0$ where $a_0 \approx 3.88$ Å is the Mn–Mn separation in the primitive perovskite cell, or on a primitive perovskite cell with a small monoclinic distortion, $a \approx c = 3.99$ Å, $b = 3.85$ Å and $b = 92^\circ$ [11, 12]. In $(La_{1-x}Ca_x)MnO_3$ above a Ca concentration of $x = 0.15$ the structure becomes cubic. An ordered superstructure is observed at $x = 0.5$ and the other end member $CaMnO_3$ of the series is indexed on a cubic cell of size $2a_0$. Intermediate compositions with $x \approx 0.1$ may be rhombohedral with $a \approx \sqrt{2}a_0$ and $a = 60.6^\circ$. A main difference between the orthorhombic, rhombohedral (trigonal) and cubic phases is the Mn-O-Mn bond angle which was refined from x-ray data to be about 150° in the orthorhombic phase, about 167° in the rhombohedral case, but 180° in the cubic case [9]. However, neutron diffraction indicated an angle of about 160° in the cubic phase [13]. The relationship between the various cells is indicated in figure 1(b).

There is now renewed interest in $(A^{3+}{}_{1-x}B^{2+}{}_x)MnO_3$ systems due to the discovery of giant negative magnetoresistance (MR) in single crystals [14] and thin films [15–20] of these materials. When the fraction of the divalent ion is about 0.3 there is a large peak in the resistivity at temperatures below the Curie point, which is associated with a metal–insulator transition. Negative magnetoresistance of over 99% [17] has been observed in thin films for applied magnetic fields > 1 T.

Structurally and chemically these manganite materials bear some resemblance to high-temperature superconductors, so experience gained in film preparation and characterization of the superconducting oxides can be applied to the manganites. This paper describes the pulsed laser deposition (PLD) and magneto-transport characterization of thin films of $(La_{1-x}Ca_x)MnO_3$ for $0 \leqslant x \leqslant 1$. The preparation and properties of the ceramic targets used in the deposition are first described, then the relation between the electronic structure of the films and that of ceramics is discussed in the final section.

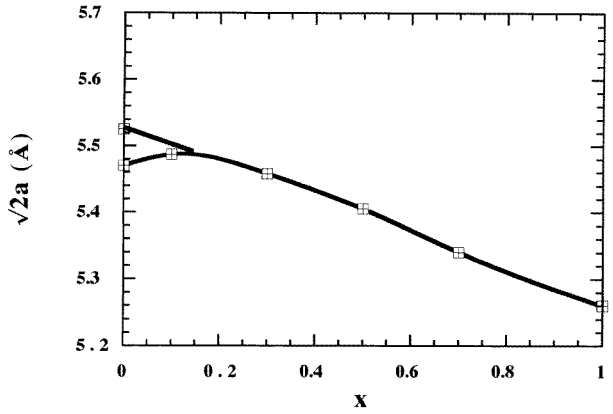

Figure 2. The lattice parameter $\sqrt{2}a_0$ as a function of x for the ceramic target materials.

2. Ceramic targets of $(La_{1-x}Ca_x)MnO_3$

2.1. Preparation and structural characterization

Ceramic targets of $(La_{1-x}Ca_x)MnO_3$, with $x = 0.0, 0.1, 0.3, 0.5, 0.7$ and 1.0, were prepared by solid state reaction of appropriate mixtures of metal oxide or carbonate powders. The mixtures were pressed into 13 mm diameter pellets and calcined at 1220 °C for 12 h in air. The ceramics were re-ground, pelletted and sintered a number of times in flowing oxygen at the same temperature. Thus dense hard targets were formed, which helps to reduce the problem of particulate contamination of laser-deposited films. x-ray diffraction was used to check the phase structure of the target materials. The crystal structure changes as the value of x increases. The phase observed depends not only on x but also on the oxygen stoichiometry [5, 9]. The manganites, although they do not show any oxygen excess, can be de-oxygenated on heating in vacuum [10], nitrogen [21] or hydrogen [5]. Following from our preparation conditions the ceramic targets are expected to have a cation deficiency of up to 5% at each of the sites [8]. In this case the structure is assigned to the rhombohedral cell. (The x-ray reflections are more conveniently indexed on the associated hexagonal unit cell.) The composition of the end member corresponds to a Mn^{4+} content of 25–30% which leads to ferromagnetic behaviour, though there are differences in the magnetic properties between the undoped (oxygen excess) and doped (stoichiometric oxygen) ferromagnetic materials [5]. The splitting of the x-ray diffraction lines disappears above a Ca concentration of $x = 0.1$ in our ceramics. The lattice parameter as a function of x is shown in figure 2. The decrease with increasing x may be related to the smaller ionic radii of Ca^{2+} and Mn^{4+}. Due to changes in the crystal structure with doping, and for convenience of interpretation, the parameters for $x > 0.1$ are given for a cubic cell ($\sqrt{2}a_0$) The $x = 0.1$ target shows a slight splitting of the 040 and 400 peak, indicating some remaining non-cubic distortion. The $x = 0.7$ sample exhibits broad lines in the diffraction pattern which might be related to charge ordering. The absence of a 110 reflection indicates that the compound may have a simple cubic (a_0, a_0, a_0) cell rather than the doubled perovskite cube of $CaMnO_3$. The degree of oxygen non-stoichiometry on doping of La for Ca is not known, though in the other studies [1, 22] a significant variation in oxygen content was observed.

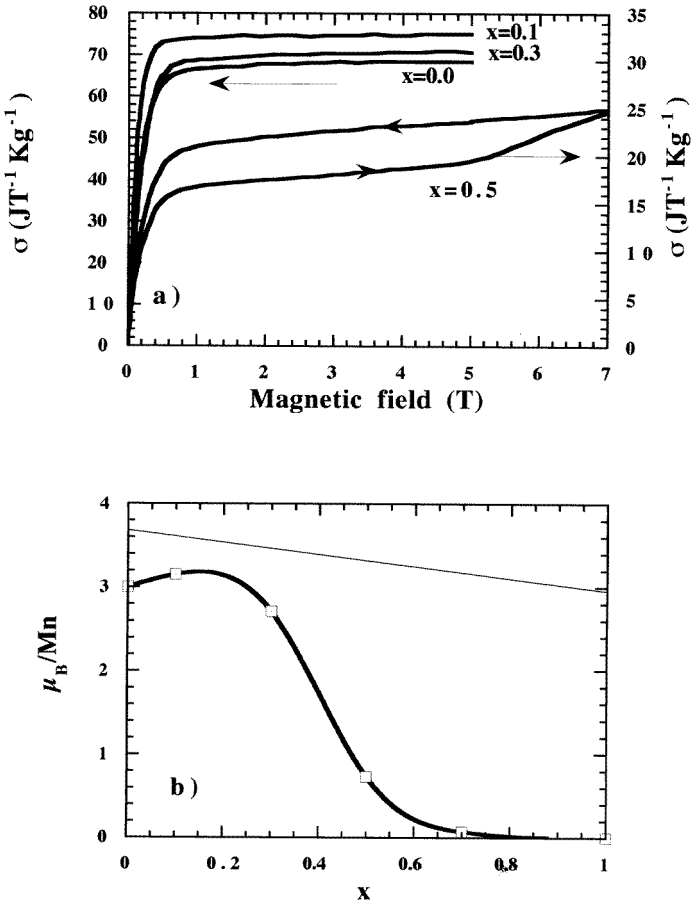

Figure 3. (a) Magnetization curves at 4.2 K for the ceramic target materials. (b) The magnetic moment per Mn atom as a function of x at 4.2 K. The straight line represents the calculated ideal ferromagnetic spin-only contribution of each Mn atom.

2.2. Magnetic properties

The ceramic powders were characterized by vibrating sample magnetometry both at room temperature and 4.2 K in a superconducting solenoid (7 T). Figure 3(a) shows the 4.2 K magnetization curves and figure 3(b) shows the magnetic moment per Mn atom as a function of x at 4.2 K, calculated from the saturation magnetization. There is a metamagnetic transition at 5 T for $(La_{0.5}Ca_{0.5})MnO_3$. Due to the cation deficiency which follows from the preparation in flowing oxygen, the end member is a ferromagnetic conductor instead of an antiferromagnetic insulator. Hence the fraction of Mn^{4+} in the ceramic ranges from 25% to 100% as x goes from 0 to 1. The straight line in figure 3(b) represents the magnetization expected for complete ferromagnetic order of the manganese spins. The magnetization measurements up to and including $x = 0.3$ show essentially ferromagnetic behaviour, although the Mn moment is reduced from its spin-only value. There could be a number of explanations for this, including an orbital contribution, covalency or a magnetic structure which is not quite collinear [4]. Above $x = 0.3$ a component of antiferromagnetic

order has been found to coexist with the ferromagnetism [7, 22].

Figure 4 shows a typical set of AC susceptibility measurements performed on long ceramic bars in the range 90–275 K. The frequency was 100 Hz and the applied field was 0.2 mT. No demagnetizing correction was made. The Curie temperatures were derived from the upper-temperature peak in the χ'' signal. The samples with $x = 0.0$ and 0.1 initially showed higher susceptibilities (χ') below the Curie temperature than did the $x = 0.3$ compound. The fall in χ' at lower temperatures and the lower temperature peak in χ'' may both be ascribed to the onset of hysteresis in excess of the applied field. The $x = 0.3$ sample develops significant hysteresis just below the Curie point.

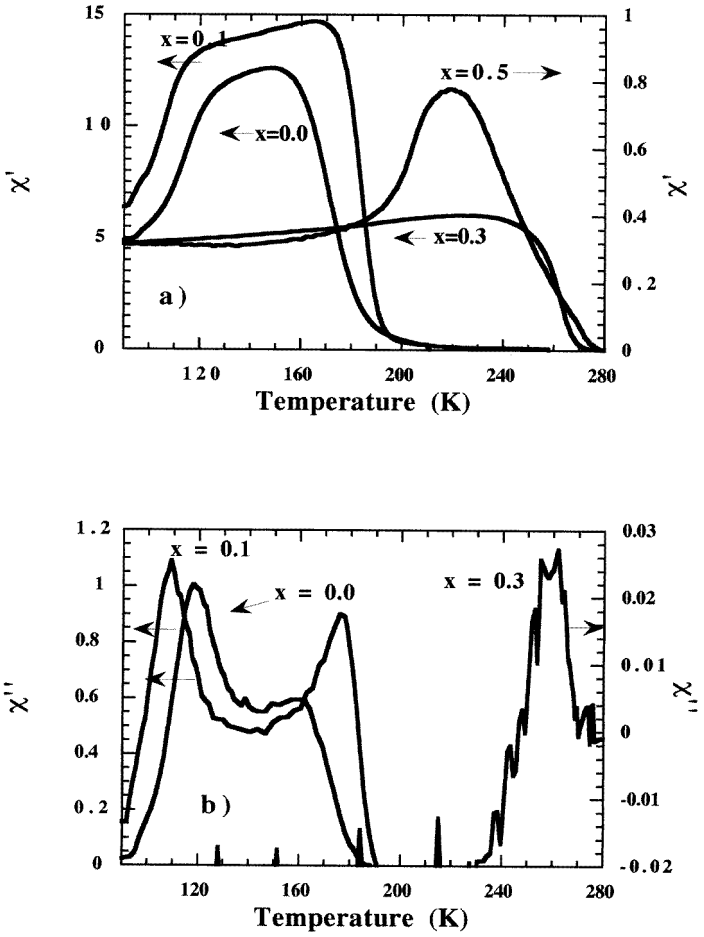

Figure 4. The AC susceptibility ((a) χ' and (b) χ'') as a function of temperature from 90–280 K for $(La_{1-x}Ca_x)MnO_3$ with $x = 0.0, 0.1, 0.3$ and 0.5.

3. Deposition and characterization of films of $(La_{1-x}Ca_x)MnO_3$

3.1. Film growth

The method used for pulsed laser deposition of manganite thin films is very similar to that for high-temperature superconductors. A KrF excimer laser operating at 248 nm, with 20 ns pulse duration and 10 Hz repetition rate, was used to ablate a ceramic target in an atmosphere of oxygen and the ablated material was condensed on a heated substrate. An aperture selects a relatively uniform part of the laser beam which was imaged, with de-magnification of 7, on to the target. The angle of incidence of the laser on the target was 30° and the area of the laser spot was 2.6 mm^2, giving a laser fluence of 1.3 J cm^{-2}. The laser beam was scanned over the target surface by rotating the target and also rotating the lens eccentrically. A heated (001) MgO substrate was placed facing the target at a distance of 4.5 cm. Oxygen was introduced through a needle valve and directed towards the substrate holder through a flexible capillary. High-quality manganite films were obtained for a substrate temperature of 720 °C and an oxygen pressure of 0.23 mbar. Optical reflectometry provided an *in situ* measure of the film thickness [23]. Figure 5 shows the variation in the reflectivity of s-polarized light at 670 nm and 29° angle of incidence during the growth of a 330 nm film of $(La_{1-x}Ca_x)MnO_3$. By fitting the measured variation in reflectivity to a theoretical calculation [23] the complex refractive index of the film at the growth conditions was found to be $2.3 - 0.5i$. Thereafter the variation in reflectivity was used to monitor the film thickness.

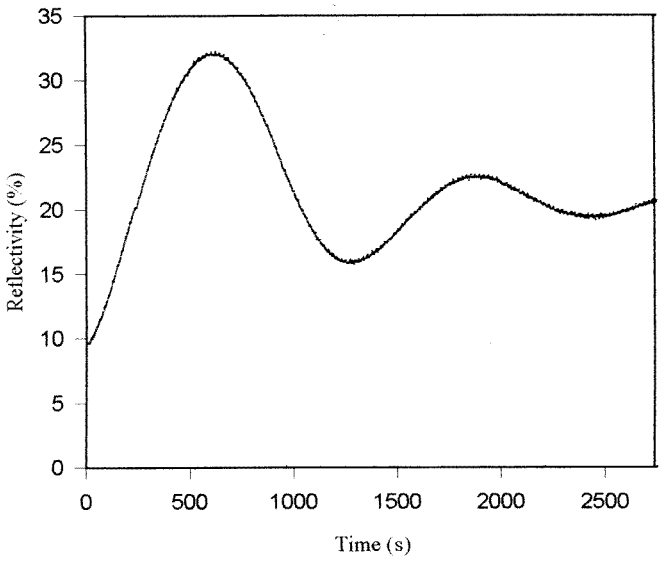

Figure 5. The variation in the s-polarized reflectivity at 670 nm and 29° angle of incidence during deposition of a 330 nm film of $(La_{1-x}Ca_x)MnO_3$ on an MgO substrate at 720 °C.

3.2. Structural and chemical characterization

The metal composition of the films was measured by energy dispersive x-ray analysis and Rutherford back-scattering (RBS). Figure 6 shows the RBS spectrum of a film prepared from

an $x = 0.3$ target. The spectrum was fitted by a 213 nm thick film with the composition $(La_{0.72}Ca_{0.30})Mn_{0.98}O_3$; assuming that there is no significant cation deficiency. This fit also shows that there is no detectable interdiffusion between the film and the substrate.

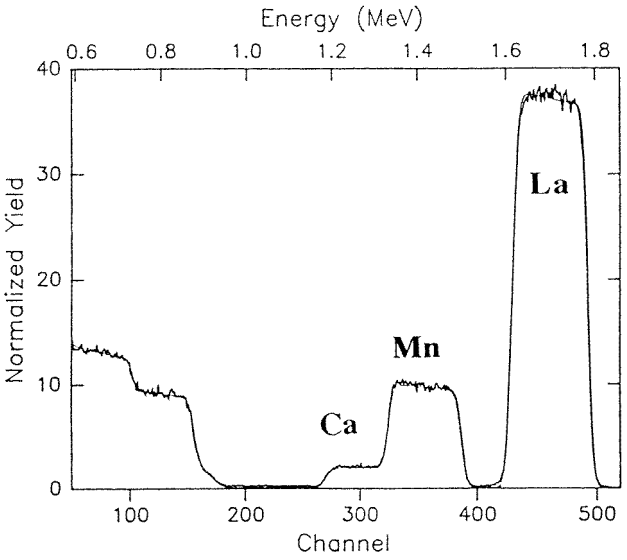

Figure 6. Rutherford back-scattering spectra of a $(La_{0.7}Ca_{0.3})MnO_3$ film which was fitted with ionic ratios of 0.72:0.3:0.97:3 and a thickness of 213 nm.

The x-ray diffraction patterns ($\theta - 2\theta$) of the series of films deposited on MgO are shown in figure 7. Like the targets, for $x \geqslant 0.1$ they are indexed on a cubic cell ($\sqrt{2}a_0$), whereas the $x = 0.0$ films are indexed on the orthorhombic cell ($\sqrt{2}a_0, \sqrt{2}a_0, 2a_0$) although only 00l lines are observed. The data indicate that the films with $x = 0$ grow with the c axis perpendicular to the plane of the substrate. The $x = 0.1$ and $x = 0.3$ films show only the $hh0$ lines of the cubic ($\sqrt{2}a_0$) structure, so in effect the orientation is the same. For $x \geqslant 0.5$ the 200 and 400 reflections are also seen, and the $x \approx 1$ $CaMnO_3$ film is ordered completely in this manner. If, for $x \leqslant 0.3$, the Mn-O-Mn bonds of the perovskite cell were ordered, for example, along the 100 axis of the MgO, then it seems that, for $x \geqslant 0.5$, the diagonal of the perovskite cell joining Mn atoms is in this direction. This is probably due to the decrease in the lattice parameters of the manganite with larger values of x. There is already a large lattice mismatch between $LaMnO_3$ and MgO (9%) and this increases for larger values of x. The lattice parameter ($\sqrt{2}a_0$) of the films as a function of x is shown in figure 8. There is an initial increase in the lattice parameter due to expansion of the c axis of the orthorhombic phase as the Jahn–Teller distortion is reduced. Above $x \approx 0.12$, for which the compound is cubic, the lattice parameter decreases linearly with increasing x. The lattice parameters of the films are slightly larger than those of the ceramic targets though the difference is largest for the $x = 0.1$ and 0.3 films; this is probably related to differences in oxygen stoichiometry, with the films lying closer to the stoichiometric composition.

3.3. Electrical properties

The resistivity (ρ) of the films was measured by the four-point van der Pauw technique. Results are shown in figure 9 on a $\log \rho$ versus $1/T$ plot. Relatively small changes in the

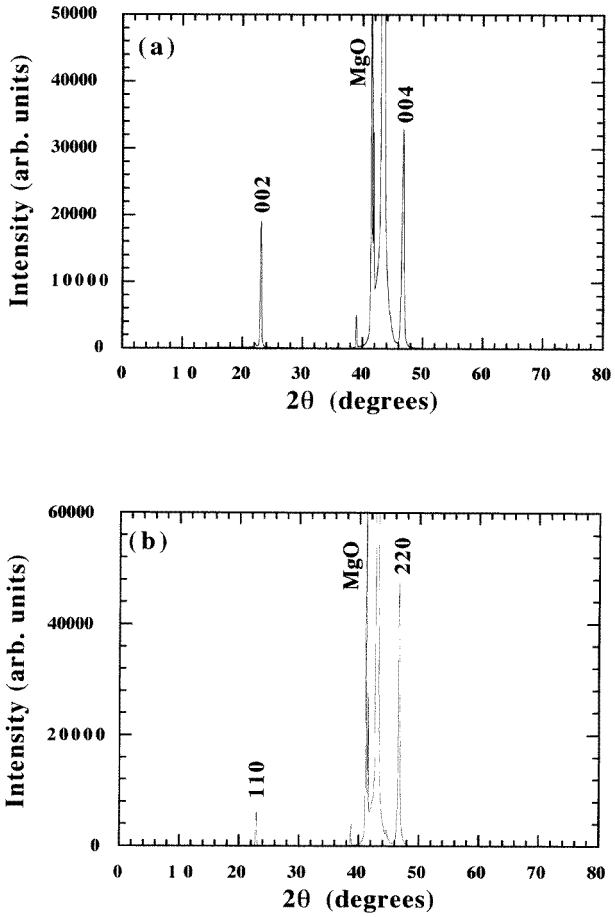

Figure 7. X-ray diffraction from films with $x = 0.0$ (a), 0.3 (b), 0.5 (c) and 1.0 (d).

Mn^{3+} : Mn^{4+} ratio modify the resistivity by several orders of magnitude. At either end of the composition range ($x = 0.0$, 0.1, 0.7 and 1.0) there is semiconductor-like behaviour. The initial activation energy for the $x = 0.0$ compound is 0.13 eV and for $x = 1.0$ it is 0.10 eV; these values drop as the temperature decreases (figure 9). Figure 10 shows the compositional dependence of the resistivity at 100 K for the films. This is similar to the behaviour of stoichiometric ceramic materials [1] and confirms that the films are close to stoichiometry. The two intermediate values ($x = 0.3$ and 0.5), which lie in the ferromagnetic composition range, show an initial increase in resistivity followed by a drop to almost metallic-like conductivity at lower temperature (about 1 mΩ cm) associated with the ferromagnetic ordering. In recent work it has been possible to sharpen the resistivity peak near T_c and reduce the residual resistivity of films with $x = 0.3$ [9, 20]. The residual resistivity is quite sensitive to crystallite size [24].

The two compositions, $x = 0.3$ and 0.5 which exhibit, in different ways, a large change in conductivity around the Curie point are also affected by the application of a magnetic field. A field of up to 0.4 T was applied in the plane of the film and parallel to the current.

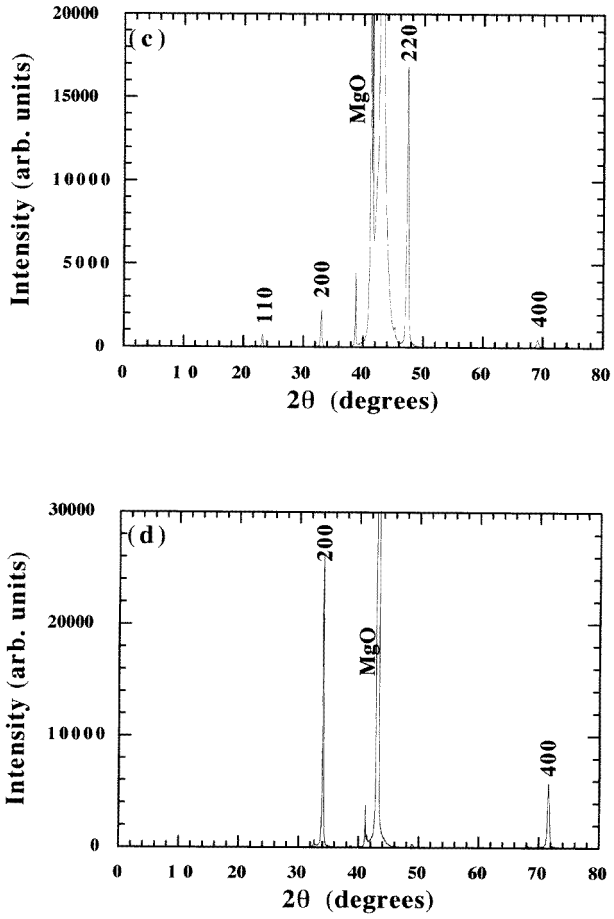

Figure 7. (Continued)

The magnetoresistance was defined as

$$\frac{\Delta\rho}{\rho_0} = \frac{\rho(B_0, T) - \rho(0, T)}{\rho(0, T)} \times 100\%$$

where $\rho(0, T)$ is the resistivity evaluated at zero field and $\rho(B_0, T)$ is the resistivity evaluated at $B_0 = 0.4$ T. Figure 11 shows the negative magnetoresistance data. The $x = 0.3$ film shows a linear decrease in the resistivity which reaches 20% using the maximum field of 0.4 T at 230 K. In the $x = 0.5$ film the negative magnetoresistance extends all the way to low temperatures, increasing monotonically as $T \to 0$. The magnitude of the maximum magnetoresistance is similar for the two compositions.

The magnetoresistance effect is due to the influence of the applied field on the spin configuration. Competition between the ferromagnetic double exchange interaction and antiferromagnetic superexchange interactions gives rise to a perturbed spin lattice in the vicinity of an electron moving in a narrow conduction band, producing partial localization and the formation of a magnetic polaron. Above the Curie point conduction may be by variable-range hopping of the magnetic polarons which gives rise to the negative temperature coefficient of resistance but below T_c the electrons in the $e_g \uparrow$ band become more or

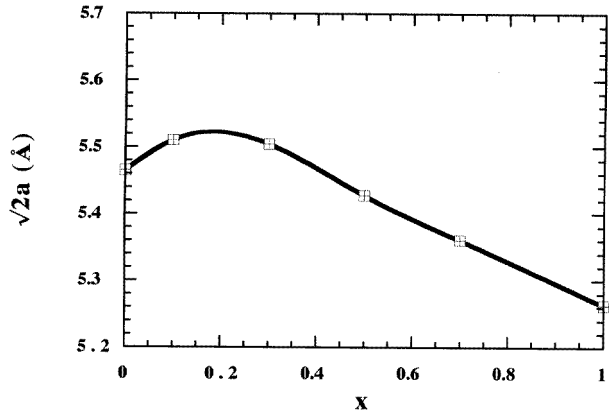

Figure 8. The variation with x of the lattice parameter ($\sqrt{2}a_0$) of the films.

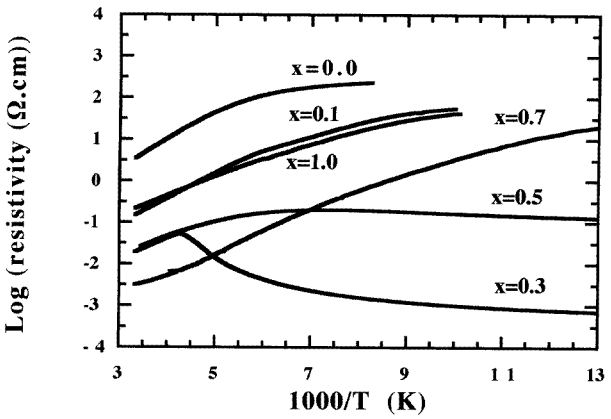

Figure 9. The resistivity as a function of temperature for manganite films with different Ca contents.

less delocalized when $x \approx 0.3$ [24]. There the ferromagnetic double-exchange interaction dominates; at low temperature the electrons are essentially delocalized and polarons can no longer be identified because the manganese ions for compositions around $x = 0.3$ are all ordered ferromagnetically. The application of a magnetic field in the vicinity of T_c increases the ferromagnetic order and reduces the spin-disorder scattering and hence the resistivity, thus producing a large magnetoresistance effect. Here ferromagnetism and conductivity are intimately related insofar as the conduction electrons are involved in the magnetic ordering process. The $x = 0.5$ film shows the magnetoresistive effect extending to low temperature since the manganese ions are never completely ferromagnetically ordered (figure 3).

The size of the magnetoresistance effect found in these films is less than those reported for films grown on $LaAlO_3$ [19] though it is similar to values in other reports, as well as for films grown on $NdGaO_3$ [26]. The latter is the substrate with the smallest lattice mismatch to $La_{0.7}Ca_{0.3}MnO_3$ (< 1%) in contrast to $LaAlO_3$ which has a larger misfit of 2%. The colossal magnetoresistance effect found in [27] appears to be due to the inclusion of an extra annealing stage. Before this treatment the films show magnetoresistance values comparable

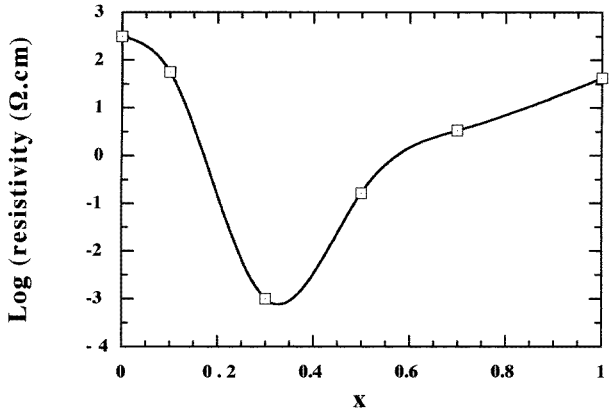

Figure 10. The composition-dependence of the resistivity of $(La_{1-x}Ca_x)MnO_3$ films at 100 K.

to our own. The exact effect of the annealing on the oxygen stoichiometry or morphology of the films remains unclear because both oxygen-rich and oxygen-deficient atmospheres are reported to improve film properties [27].

4. Optical properties

The optical transmission spectra of the $x = 0.0, 0.3$ and 0.5 films are shown in figure 12. The main absorption edge, deduced from plots of α^2 versus $h\nu$, is at 3.1, 3.0 and 2.55 eV respectively. It is associated with 2p(O) $\rightarrow$ 3d(Mn) charge transfer [28]. The second structure in the transmission spectra is the absorption band in the red. For $(La_{0.7}Ca_{0.3})MnO_3$, two features can be distinguished, at 1.5 and 2.2 eV. The same features appear in the spectrum of $LaMnO_3$, for which they lie about 0.2 eV higher, whereas for $x = 0.5$ only one feature is visible. These absorptions are probably due to Mn d $\rightarrow$ d transitions [29]. The presence of two distinct absorptions in the $x = 0.0$ and 0.3 compositions is due to Jahn–Teller distortion, this becomes more dynamic with increasing x and is no longer evident in the $x = 0.5$ composition. The Jahn–Teller splitting of the e_g levels of Mn^{3+} in soilds is typically ≈ 1 eV [30].

The Faraday effect was measured in the wavelength range 390–940 nm and the temperature range 15–300 K. The analyser was oriented at 45° to the polarizer for maximum sensitivity. The transmission spectrum in zero field was subtracted from the spectrum in a field of 0.4 T applied perpendicular to the plane of the sample and in the direction of the light. Since the magnetizations $\mu_0 M$ of the $x = 0.3$ and 0.5 compounds are 0.55 and 0.18 T, respectively, the applied field is almost sufficient to saturate the Faraday signal. In the Faraday spectrum, figure 13, there are two spectral regions with strong magneto-optic activity below the Curie temperature corresponding roughly to the two structures in the absorption spectra. The Faraday spectra give Curie temperatures of 220 ± 10 and 280 ± 10 K for the $x = 0.3$ and 0.5 films respectively. There is also an appreciable Faraday effect in the region of 1.8 eV and beyond. For example at 830 nm, θ_F is 10000 °/cm and $\alpha = 1.5 \times 10^5$ cm^{-1} for the $x = 0.3$ sample, giving a figure of merit $\theta_F/\alpha = 0.13$. Further details of the absorption measurements and their interpretation may be found in [28].

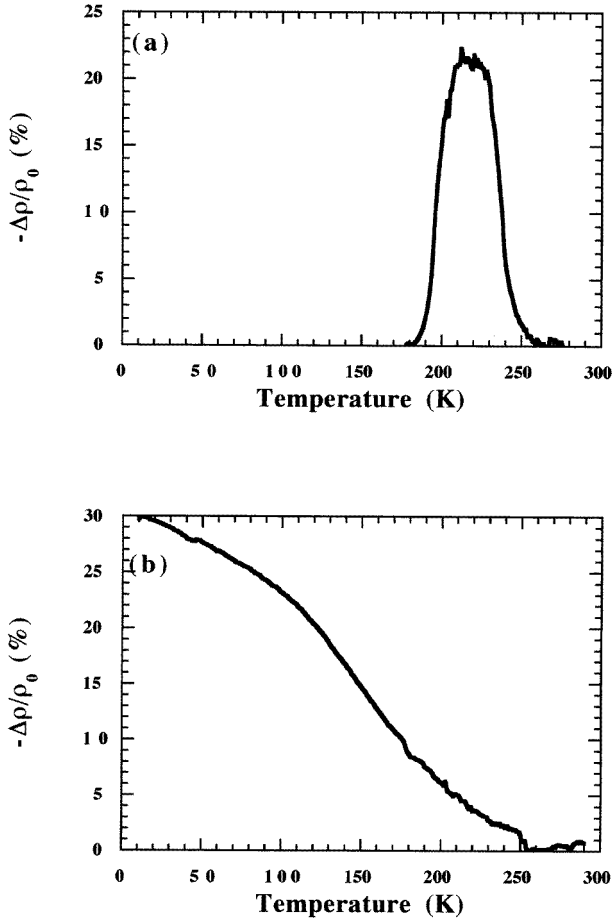

Figure 11. The magnetoresistance at 0.4 T as a function of temperature for (a) the $x = 0.3$ film and (b) the $x = 0.5$ film.

5. Conclusions

We have shown that high-quality oriented films of the entire $(La_{1-x}Ca_x)Mn)O_3$ series can be prepared by PLD using conditions similar to those for copper oxide superconductors. By using heated substrates in a low oxygen pressure it is possible to obtain films which are closer to stoichiometry than are the ceramic targets. Optical reflectivity provides a convenient technique for *in situ* monitoring of the film growth.

The films exhibit physical properties similar to those of high-quality ceramics, namely a maximum low-temperature conductivity at $x \approx 0.3$ which approaches the minimum metallic conductivity and coincides with the existence of ferromagnetic order, shown by the Faraday effect measurements.

The negative magnetoresistance effect is qualitatively different for the $x = 0.3$ and 0.5 films. For $x = 0.3$ the MR peak occurs in the vicinity of the Curie point, as determined by magneto-optic measurements on the same sample. However, for $x = 0.5$ the onset of magnetoresistance is a little below T_c and the effect does not peak at any temperature, but

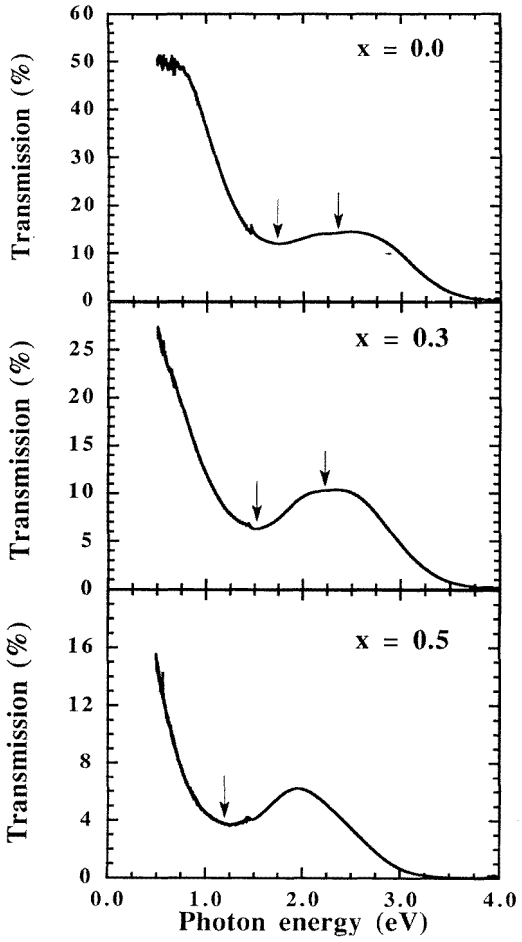

Figure 12. Optical transmission spectra for 200 nm films of $(La_{1-x}Ca_x)MnO_3$ with $x = 0.0$, 0.3 and 0.5.

increases monotonically as $T \to 0$. This may be interpreted as showing that the applied field modifies the magnetic order (on the scale of the spin diffusion length) down to the lowest temperatures for $x = 0.5$, but for $x = 0.3$ the ferromagnetic order is essentially complete and collinear below the Curie point. It is only in the vicinity of T_c, at which the 3d $\uparrow$ electrons in the σ^* conduction band begin to be localized by magnetic disorder, that a large negative magnetoresistance appears. In other words, the spin configuration is field-sensitive at all temperatures less than T_c for $x = 0.5$, but only near T_c for $x = 0.3$.

Finally we note that the Faraday effect in the region 1.5–2.0 eV which is associated with d–d transitions ($^5E_g \to {}^5T_{2g}$ of the $3d^4$ Mn^{4+} ion [27]) peaks about 30 K below T_c both for $x = 0.3$ and for $x = 0.5$. There may be a connection between the magnitude of the magneto-optic effect and the charge-transfer frequency on an optical timescale, but this point requires further investigation.

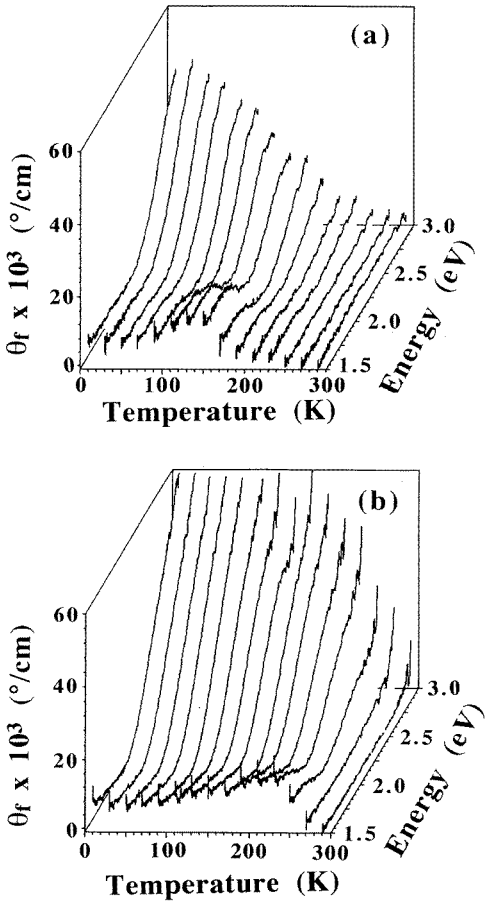

Figure 13. The Faraday rotation as a function of wavelength over the temperature range 10–290 K for films of $(La_{1-x}Ca_x)MnO_3$ with compositions (a) $x = 0.3$ and (b) $x = 0.5$.

Table 1. A summary of the magnetic properties of the target materials as determined by vibrating sample magnetometry and AC susceptibility.

Target	σ (J T^{-1} kg^{-1})	Mn moment (μ_B)	T_C (K)	T_N (K)
$x = 0.0$	68.4	3.00	158	
$x = 0.1$	75.1	3.15	174	
$x = 0.3$	70.7	2.71	265	
$x = 0.5$	21	0.73	225	
$x = 0.7$	2.0	0.07		140
$x = 1.0$	0.0	0.0		145

Acknowledgments

The optical monitoring of the film growth was performed by Rory Jordan. The RBS measurements were performed by Laurent Ranno of the Groupe de Physique du Solide, Université Pierre et Marie Curie, Paris VI. The authors also wish to acknowledge the help

of Michel Viret in the preparation of this paper. This work was partially supported by the EU under the ALADIN project on PLD in the Brite/Euram programme. The work on magnetic thin films was supported by Forbairt, the Irish science and technology agency.

References

[1] Jonker G H and van Santen J H 1950 *Physica* **16** 337
[2] Zener C 1951 *Phys. Rev.* **82** 403
[3] Anderson P W and Hasegawa H 1995 *Phys. Rev.* **100** 675
[4] de Gennes P G 1960 *Phys. Rev.* **118** 141
[5] Ranno L, Viret M, Mari A, Thomas R M and Coey J M D 1996 *J. Phys.: Condens. Matter* **7** L1
[6] Goodenough J B 1955 *Phys. Rev.* **100** 564
[7] Matsumoto G 1970 *J. Phys. Soc. Japan* **29** 606
[8] van Roosemalen and Cordfunke E H P 1994 *J. Solid State Chem.* **110** 106
[9] Hervieu M, Mahesh R, Rangavittal N and Rao C N R 1995 *Eur. J Solid State Inorg. Chem.* **32** 79
[10] Kuo J H, Anderson H V and Sparlin D M 1989 *J. Solid State Chem.* **83** 52
[11] Jonker G H 1956 *Physica* **22** 707
[12] Matsumoto G 1970 *J. Phys. Soc. Japan* **29** 615
[13] Hwang H Y, Cheong S W, Radaelli P G, Marezio M and Batlogg B 1995 *Phys. Rev. Lett.* **75** 914
[14] Searle C W and Wang S T 1970 *Can. J. Phys.* **48** 2023
[15] Cho J, Gomi M and Abe M 1990 *Japan. J. Appl. Phys.* **29** 1686
[16] von Helmolt R, Wecker J, Hopzapfel B, Schultz L and Samwer K 1993 *Phys. Rev. Lett.* **71** 2331
[17] Jin S, Tiefel T H, McCormack M, Fastnacht R A, Ramesh R and Chen L H 1994 *Science* **264** 413
[18] Lawler J F and Coey J M D 1995 *J. Magn. Magn. Mater.* **140–144** 2049
[19] Xiong G C, Li Q, Ju H L, Mao S N, Senapati L, Xi X X, Greene R L and Venkatesen T 1995 *Appl. Phys. Lett.* **66** 1427
[20] Xiong G C, Li Q, Ju H L, Greene R L and Venkatesan T 1995 *Appl. Phys. Lett.* **66** 1689
[21] Pauthenet R and Veyret C 1970 *J. Physique* **31** 65
[22] Wollan E O and Koehler W C 1955 *Phys. Rev.* **100** 545
[23] Jordan R, McConnell M and Lunney J G 1995 *Supercond. Sci. Technol.* **8** 504
[24] Gupta A, Gong G Q, Gang X, Duncombe P R, Lecoeur P, Trouilloud P, Wang Y Y, Dravid V P and Sun J Z to be published
[25] Coey J M D, Viret M, Ranno L and Ounadjela K 1995 *Phys. Rev. Lett.* **75** 3910
[26] Zeng X T and Wong H K 1995 *Appl. Phys. Lett.* **66** 3371
[27] Ju H L, Kwon C, Li Q, Greene R L and Venkatesan T 1994 *Appl. Phys. Lett.* **65** 2108
[28] Lawler J F, Lunney J G and Coey J M D 1994 *Appl. Phys. Lett.* **65** 3017
[29] Subba Rao G V, Rao C N R, and Ferraro J R 1970 *Appl. Spectrosc.* **24** 436
[30] Burns R G 1993 *Mineralogical Applications of Crystal Field Theory* 2nd edn (Cambridge: Cambridge University Press)